

Ultrafast L Band Soliton Pulse Generation in Erbium-Doped Fiber Laser Based on Graphene Oxide Saturable Absorber

Hazlihan Haris ^{1,*}, Malathy Batumalay ^{2,*} , Tan Sin Jin ³, Ahmad Razif Muhammad ⁴ , Arni Munira Markom ⁵, Caroline Livan Anyi ⁶, Muhamad Hakim Izani ⁴, Mohd. Zulkhimi Ab. Razak ⁴ , Megat Muhammad Ikhsan Megat Hasnan ¹  and Ismail Saad ^{1,*}

¹ Faculty of Engineering, Universiti Malaysia Sabah (UMS), Kota Kinabalu 88400, Malaysia

² Faculty of Data Science & IT, INTI International University, Nilai 71800, Malaysia

³ School of Engineering, UOW Malaysia KDU University College, Shah Alam 40150, Malaysia

⁴ Institute of Microengineering and Nanoelectronics (IMEN), Universiti Kebangsaan Malaysia (UKM), Bangi 43600, Malaysia

⁵ School of Electrical Engineering, College of Engineering, Kampus Pasir Gudang, Universiti Teknologi MARA, Masai 81750, Malaysia

⁶ School of Chemistry, Chemical Engineering and Biotechnology, Nanyang Technological University, 62 Nanyang Dr, Singapore 637459, Singapore

* Correspondence: hazlihanharis@ums.edu.my (H.H.); malathy.batumalay@newinti.edu.my (M.B.); ismail_s@ums.edu.my (I.S.)

Abstract: We demonstrate a simple mode-locked Erbium-doped fiber laser (EDFL) based on self-synthesized saturable absorber (SA) by combining graphene oxide (GO) and polyethylene oxide (PEO) solutions to form a GO-PEO thin film. This thin film was incorporated into an Erbium-doped fiber laser (EDFL) with a cavity length of 9 m. Our EDFL could operate at a 22 MHz repetition rate with a 0.8 ps pulse duration. The laser also showed stable soliton pulses under various laser pump power values. Our reported results show that GO-PEO SA is effective and proven as a cost-effective material for saturable absorbers for EDFLs.

Keywords: EDFL; pulsed fiber laser; saturable absorber; graphene oxide



Citation: Haris, H.; Batumalay, M.; Jin, T.S.; Muhammad, A.R.; Markom, A.M.; Anyi, C.L.; Izani, M.H.; Razak, M.Z.A.; Megat Hasnan, M.M.I.; Saad, I. Ultrafast L Band Soliton Pulse Generation in Erbium-Doped Fiber Laser Based on Graphene Oxide Saturable Absorber. *Crystals* **2023**, *13*, 141. <https://doi.org/10.3390/cryst13010141>

Academic Editor: Yuri Kivshar

Received: 13 December 2022

Revised: 29 December 2022

Accepted: 1 January 2023

Published: 13 January 2023



Copyright: © 2023 by the authors. Licensee MDPI, Basel, Switzerland. This article is an open access article distributed under the terms and conditions of the Creative Commons Attribution (CC BY) license (<https://creativecommons.org/licenses/by/4.0/>).

1. Introduction

The first report of ultra-short pulses' generation from passively mode-locked fiber lasers by incorporating graphene-based saturable absorbers (SA) was made more than a decade ago [1]. Since then, various fiber laser configurations have been proposed, utilizing erbium-doped fibers (EDFL) [2–6]. EDFLs are sought after, as they offer various applications in many industrial and scientific research areas, such as biomedical imaging research, material processing, and supercontinuum generation [7–9]. Nowadays, despite a growing number of SAs based on new materials, such as the Topological Insulator [10,11], Transition Metal Dichalcogenides (TMD) [12], Black Phosphorus [13,14], MXenes [15,16], metal halide perovskites [17], ferromagnetic semiconductors [18], and Ternary Transition Metal Chalcogenides (TTMC) [19] having emerged, graphene is still irreplaceable by new materials due to its fascinating saturable absorption properties and broad operational wavelength range. More recently, much research has begun to focus on graphene oxide material and its various applications in photonics [20–22]. Graphene oxide is an atomically thin sheet of carbon bonded with oxygen functional groups, which can be produced by the oxidative treatment of graphite [23]. Hence, as a by-product, graphene oxide is cheaper and more easily accessible than graphene. Moreover, the covalent oxygen functional groups in graphene oxide not only represent strong hydrophilic properties, but also create a remarkable mechanical strength that offers a superior flexibility and processibility for the production of graphene-oxide-based optoelectronics [24]. Further investigation shows that graphene oxide has an ultrafast recovery time and strong saturable absorption, which is

comparable to that of graphene [25]. Some remarkable works on pulsed fiber lasers with GO were reported. Sobon et al. observed a soliton pulse at a 1558 nm wavelength and an FWHM bandwidth as broad as 9.3 nm [26]. Xu et al. modified the laser cavity dispersion to -0.008 ps^2 , and this resulted in a narrow pulse width at 0.2 ps [20]. They reported pulsing a very low pulsing threshold power of 27 mW. In this paper, we demonstrate observing soliton in a mode-locked EDFL by employing graphene oxide embedded into PEO film as passive SA. The fabricated GO film had a nonlinear saturable absorption or modulation depth of 24.1%, and it was integrated into an EDFL cavity to produce soliton pulses. The EDFL operates in the L-band region, with a center wavelength of 1565.2 nm with stable mode-locking states between pump powers of 39.0 to 170.2 mW. We would like to highlight that our work generates a soliton pulse in the L-band region with a high fundamental frequency of 22 MHz and that its performance is comparable to the work demonstrated by others. This will provide an alternative to the exhausted C-band transmission capability. Additionally, the recorded pump threshold power required to initiate mode-locking is low, at 39 mW. The sub-picoseconds pulse is attractive for expanded L-band terrestrial Dense Wavelength Division Multiplexing (DWDM) and submarine optical communication networks.

2. Synthesis and Characterization of GO-PEO Film as Saturable Absorber

We synthesized the GO used in this work by using a modified Hummers method [27]. Firstly, we mixed 320 mL of sulfuric acid and 80 mL of phosphoric acid, together with 18 g of graphite flakes and 20 g of potassium permanganate, by using a magnetic stirrer. After the mixture was combined thoroughly, it was left to stir for 72 h to allow for the oxidation of graphite to occur. This is implied by the mixture's color change from dark purplish green to dark brown. Then, we added hydrogen peroxide solution to stop the oxidation process. Here, the color of the mixture switched to bright yellow, indicating a high oxidation level of graphite.

The formed GO was then rinsed at least three times with 1 M of hydrogen chloride aqueous solution, followed repeatedly by deionized water, until a pH of 4–5 was achieved. This washing process was performed using a simple decantation of supernatant via a centrifugation technique, with a centrifugation force of $10,000 \times g$. During the washing process, the GO experienced exfoliation, resulting in the thickening of the graphene solution, forming a GO gel. Finally, the GO gel was mixed with deionized water to obtain a graphene oxide solution.

We prepared the polymer by dissolving 1 g polyethylene oxide (PEO) with 120 mL of deionized water, using a hot plate stirrer with the aid of a magnetic stirrer. The PEO took approximately three hours to become fully dissolved in DI water. We fabricated GO-PEO composites by adding a different quantity of dispersed GO suspension containing GO into a solution of 1 g PEO in deionized water and stirred thoroughly via an ultra-sonification process. Next, the solution was placed into an ultra-sonic bath (Branson 2510, 40 kHz, Branson Ultrasonics, Shanghai, China) for about one hour to produce a stable GO-PEO composite solution. Lastly, this concoction of PEO and GO was dried at room temperature to obtain a GO-PEO film. The dried GO-PEO film is shown in Figure 1a.

Figure 1b is the Field Emission Scanning Electron Microscope (FESEM) image of the fabricated GO (500 nm in dimension). The figure shows well-defined and interconnected graphene sheets forming a porous and loose sponge-like structure. Figure 1c shows the Raman spectra of the synthesized GO, displaying a D peak at 1359 cm^{-1} and a G peak at 1600 cm^{-1} . The observation of the D band is due to the defect-induced breathing mode of sp^2 rings. On the other hand, the depiction of the G band is caused by first-order scattering of the E_{2g} phonon of sp^2 carbon atoms, respectively [28,29]. As observed, the G band of the GO is located at a higher frequency compared to graphite, which is at 1580 cm^{-1} . This observation corresponds well with the finding reported in [30]. The (I_D/I_G) intensity ratio for GO is computed at 0.85, which is the measure of the disorder degree and is inversely proportional to the average size of the sp^2 clusters [26]. Figure 1d displays the measured

nonlinear transmission curve of the GO-PEO film. As shown, the film exhibits a 24.1% nonlinear saturable absorption, as well as a modulation depth of 72 MW/cm² saturable intensity and a 35.1% non-saturable absorption.

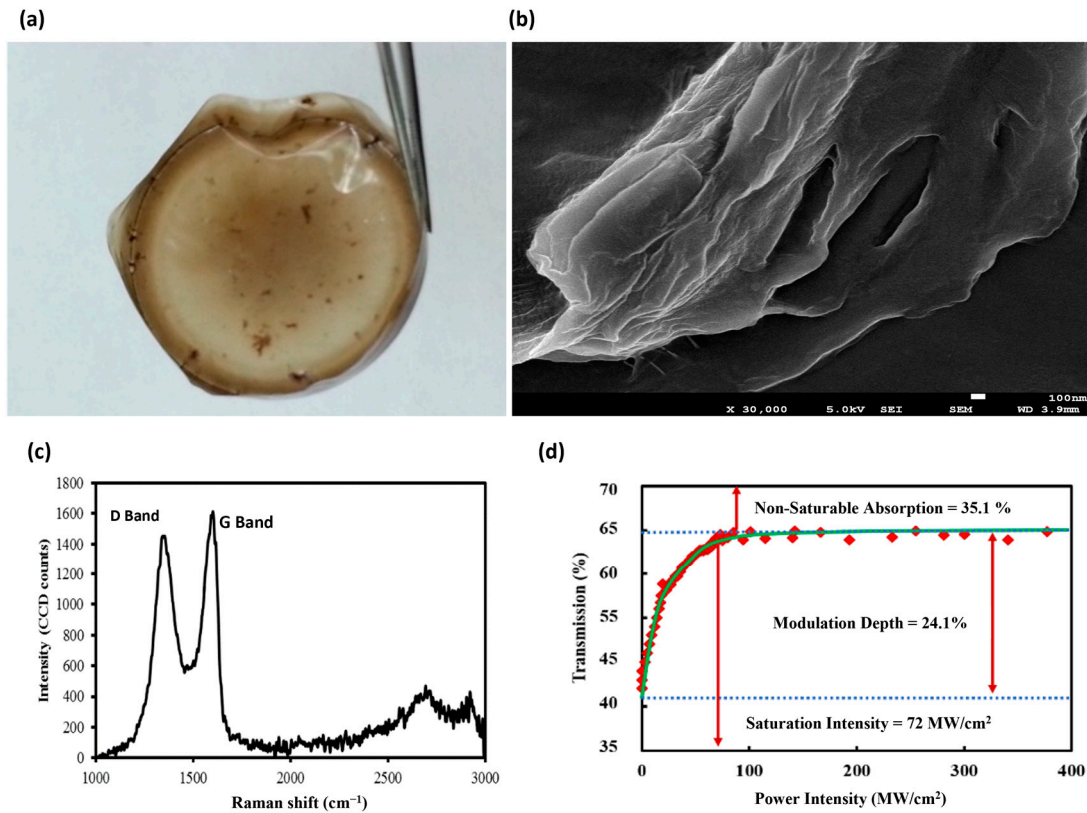


Figure 1. Fabrication and characterization of GO-PEO film: (a) GO-PEO film after letting it dry at room temperature; (b) FESEM image of GO-PEO film; (c) Raman spectrum from the GO-PEO film; (d) Modulation Depth of the GO-PEO film.

3. Generation of Soliton Pulses with GO-PEO Film as Saturable Absorber

The prepared GO-PEO film was cut into small pieces. A ready-made piece of it was attached to an FC/PC fiber ferrule with index matching gel, as shown in Figure 2 labelled with “GO-SA”. We then matched this ferrule with another fresh ferrule via an adaptor. The insertion loss of the SA was measured as being around 1.5 dB at 1550 nm. The EDFL has a total cavity length of 9 m: 3 m long EDF as the gain medium, 0.6 m wavelength division multiplexer (WDM) fiber, and 5.4 m long SMF, with a group velocity dispersion (GVD) of 21.6 ps²/km, −38.0 ps²/km, and −21.9 ps²/km, respectively, at 1550 nm. To complete a ring cavity laser configuration, a 980 nm laser diode was used to pump the EDF via 980/1550nm (WDM) and directly spliced to unidirectional isolator. A 90:10 coupler was used to extract the 10% of total laser’s intracavity beam for a spectrum and performance evaluation via optical measurement devices. The cavity operates in an anomalous fiber dispersion of −0.20 ps², and thus traditional soliton tends to be formed in the fiber laser.

The laser generated a stable mode-locking pulses train, owing to the balance between the GVD and nonlinearity effect within the ring cavity. Continuous wave (CW) lasing was firstly observed at around a 32 mW pump power, and it subsequently changed to a mode-locked operation when the pump power was increased to 39.3 mW. The mode-locking operation was maintained as the pump power was further increased to 170.2 mW. We also confirmed that without the insertion of the GO-PEO film, no pulsing was detected. This proved that the establishment of the pulsing operation was purely contributed to by our fabricated GO-PEO SA.

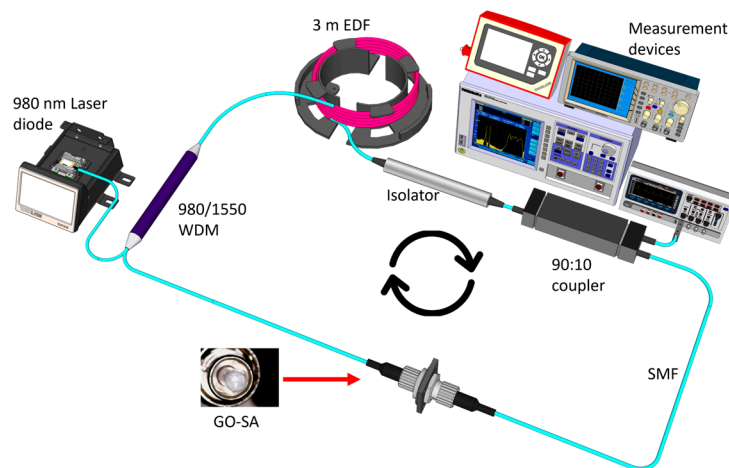


Figure 2. Configuration of the mode-locked EDFL with GO-PEO film-based SA consist of 980nm laser diode, 980/1550 nm WDM, 3 m EDF, isolator, 90:10 coupler, measurement devices, SMF and GO-SA thin film.

Figure 3a illustrates the optical spectrum of the mode-locked EDFL at a pump power of 110.8 mW. The spectrum is centered at 1565.2 nm with a 3 dB bandwidth of 5.6 nm. Kelly sidebands are also noticeably observed on both sides of the spectrum, demonstrating that the mode-locked operation was in the anomalous dispersion soliton regime. The formation of Kelly sidebands is due to periodic perturbations in the laser cavity. The interaction between dispersion and nonlinearity in the ring cavity produces a good generation of soliton pulses. Figure 3b shows a typical oscilloscope trace at a 110.8 mW pump power, which indicates a stable mode-locked pulse. We noticed that the pulse train is uniform with slightly distinct amplitudes for each envelope spectrum due to the effect of birefringence in fiber. When the soliton pulse intensity is strong, the pulse evolves nonlinearly at both orthogonal axes of the fiber. The interaction between these two orthogonal axes resulted in a non-uniform pulse train. The distance of the peak-to-peak oscillation of the pulse train is measured to be 45.4 ns, as shown in the inset of the zoomed-in view of the pulse train in Figure 3b. This corresponds to a repetition rate of 22 MHz, which agrees well with the cavity length of about 9 m.

Figure 3c illustrates the pulse width measurement with a secant hyperbolic-fitting curve autocorrelation trace. The pulse duration was measured to be 0.8 ps, and the time-bandwidth product (TBP) was 0.52, which was slightly higher than the value of 0.315 of transform-limited sech^2 pulses. This suggests that the optical pulse is slightly chirped. The RF spectrum of the laser is depicted in Figure 3d. The fundamental cavity frequency was 22 MHz (corresponding to the cavity round-trip time, 45.4 ns). The electrical signal-to-noise ratio (SNR) was 35.8 dB, demonstrating that the mode-locking state was stable.

We varied the pump power to validate the laser's stability and discovered that the mode-locking state could be maintained within pump power ranges of 39.3 to 170.2 mW. We also observed that the mode-locking operation became unstable and disappeared when the pump power was increased beyond 170.2 mW. Figure 4 shows the relationship between the output average power, indicated by blue-dotted lines and single pulse energy with respect to the incident pump power which indicated by red-dotted lines. We found that both the output power and pulse energy increase monotonously with the pump power. At a maximum pump power of 170.2 mW, the average output power and pulse energy were measured to be 3.37 mW and 0.153 nJ, respectively. Pulsing is still present when the pump power is raised to the maximum available power at 170.2 mW. Therefore, it can be concluded that the damage threshold is beyond 170.2 mW. Compared to the previous graphene-based mode-locked laser, our GO-PEO-based laser produced a slightly higher output power and pulse energy [31].

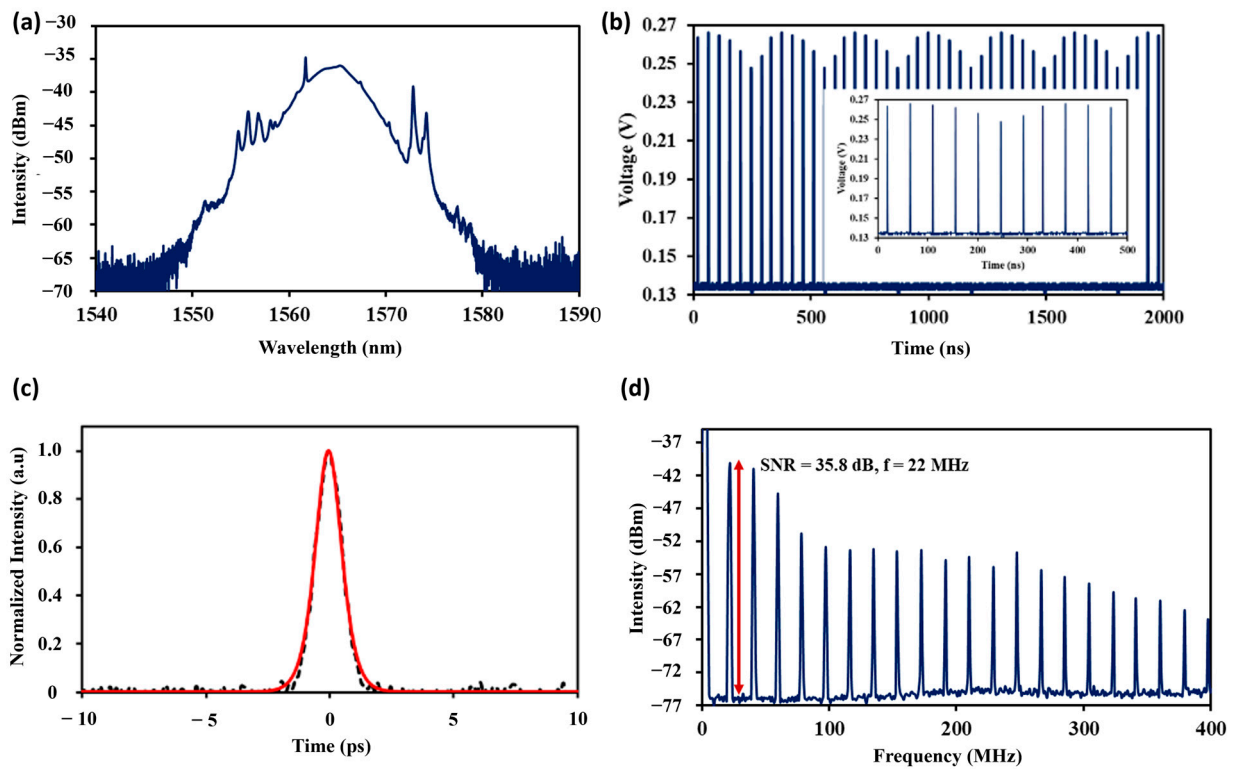


Figure 3. (a) Characteristics of the soliton mode-locked pulse at pump power of 110.8 mW; (a) optical spectrum at OSA; (b) typical pulse train at oscilloscope; (c) pulse width measurement with auto-correlator trace; (d) RF spectrum with RF spectrum analyzer.

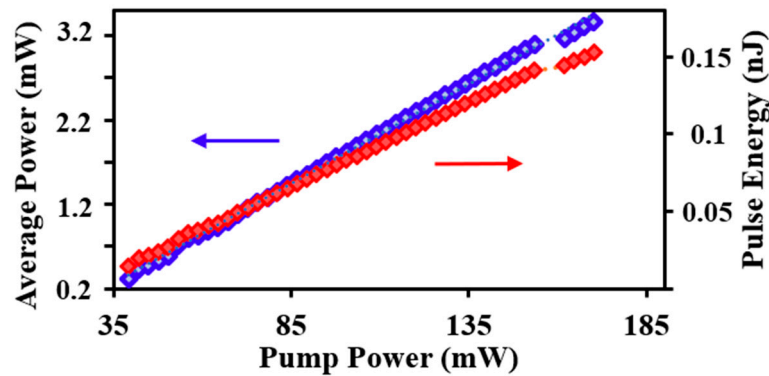


Figure 4. Average output power and pulse energy against pump power for the GO-PEO-based mode-locked soliton EDFL.

Table 1 below summarizes some work on the mode-locked pulsed fiber laser at the C- and L-band regions based on GO SA. The performance of our mode-locked fiber laser cavity is comparable to others. Even though a low threshold power was reported in [20], when the power increased beyond 69 mW, the single pulse broke into multiple pulses. Our mode-locked fiber laser is emitting in the L-band region, with a low threshold power and high repetition rate. The L-band emission can provide capacity enhancement to the backbone of the optical network. Throughout the variation of pump power from 39 mW to 170.2 mW, the laser emission is stable at its fundamental repetition rate.

Table 1. Summary of work on mode-locked pulsed fiber laser covering C- and L-band regions using GO SA.

Integration Method	Repetition Rate	Pulse Width	Threshold Pump Power	Pulse Profile, Pulse Center Wavelength and 3 dB Bandwidth	Maximum Output Power	Ref
Fiber ferrule	21.79 MHz	770 fs	98 mW	Soliton, 1596 nm, 4.454 nm	0.85 mW	[32]
Mirror	19.5 MHz	11 ps	139 mW	Dissipative soliton, 1531 nm, 6.5 nm	2.23 mW	[33]
D-shape fiber	14.64 MHz	780 fs	162 mW	Soliton, 1555.9 ns, 3.73 nm	0.36 mW	[34]
Fiber ferrule	9.4 MHz (fundamental) 37.7 MHz (Harmonic)	1.2 ps 1.2 ps	80 mW	Soliton, 1571 nm, 3.9 nm Soliton, 1560 nm, 4.8 nm	-	[35]
Photonic Crystal Fiber	7.68 MHz (fundamental) 76.8 MHz (Harmonic)	4.83 ns	38 mW	Dissipative soliton, 1561.2 nm, 0.11 nm	4.3 mW	[36]
Fiber ferrule	40.32 MHz	750.5 fs	80 mW	Soliton, 1559.60 nm, 3.8 nm	-	[37]
Mirror	22.9 MHz	0.2 ps	27 mW	Soliton, 1560 nm	5.8 mW	[20]
Fused silica plates	58 MHz	390 fs	92 mW	Soliton, 1558 nm, 9.3 nm	1.96 mW	[26]
Fiber ferrule	13.9 MHz	0.6 ps	78 mW	Soliton, 1577.46 nm, 5.4 nm	38.1 uW	[38]
Fiber ferrule	22 MHz	0.8 ps	39.0 mW	Soliton, 1565.2 nm, 5.6 nm	3.37 mW	This work

4. Conclusions

In conclusion, we successfully demonstrate a soliton-mode-locked EDFL using GO-PEO SA. The EDFL operates at a center wavelength of 1565.2 nm and generates a repetition rate of 22 MHz with stable soliton pulses at a duration of 0.8 ps. The EDFL can output a maximum average power range of 3.37 mW with a maximum pulse energy calculated at 0.153 nJ. This work demonstrates that self-synthesized GO-PEO SA is suitable to be utilized as a simple and low-cost SA for ultrashort pulse generation in the L-band region.

Author Contributions: Conceptualization, methodology and validation, formal analysis, writing—original draft preparation, H.H., M.B., I.S., A.R.M. and T.S.J.; resources, I.S.; formal analysis, M.M.I.M.H. and M.H.I.; writing—review and editing, A.M.M.; visualization, A.R.M., C.L.A. and M.Z.A.R.; supervision, I.S.; project administration and funding acquisition, I.S. All authors have read and agreed to the published version of the manuscript.

Funding: This research was funded by Niche Research Fund Scheme, Universiti Malaysia Sabah (UMS), grant number SDN00286 and Postgraduate Research Grant Scheme (UMSGreat), grant number GUG0444-1/2020. The APC was funded by I.S.

Institutional Review Board Statement: Not applicable.

Informed Consent Statement: Not applicable.

Data Availability Statement: Not applicable.

Conflicts of Interest: The authors declare no conflict of interest.

References

1. Bao, Q.L.; Zhang, H.; Wang, Y.; Ni, Z.H.; Yan, Y.L.; Shen, Z.X.; Loh, K.P.; Tang, D.Y. Atomic-Layer Graphene as a Saturable Absorber for Ultrafast Pulsed Lasers. *Adv. Funct. Mater.* **2009**, *19*, 3077–3083. [[CrossRef](#)]
2. Sobon, G.; Sotor, J.; Pasternak, I.; Krajewska, A.; Strupinski, W.; Abramski, K.M. Multilayer graphene-based saturable absorbers with scalable modulation depth for mode-locked Er-and Tm-doped fiber lasers. *Opt. Mater. Express* **2015**, *5*, 2884–2894. [[CrossRef](#)]
3. Zhang, H.; Bao, Q.L.; Tang, D.Y.; Zhao, L.M.; Loh, K. Large energy soliton erbium-doped fiber laser with a graphene-polymer composite mode locker. *Appl. Phys. Lett.* **2009**, *95*, 141103. [[CrossRef](#)]
4. Popa, D.; Sun, Z.; Torrisi, F.; Hasan, T.; Wang, F.; Ferrari, A.C. Sub 200 fs pulse generation from a graphene mode-locked fiber laser. *Appl. Phys. Lett.* **2010**, *97*, 203106. [[CrossRef](#)]
5. Sun, Z.; Hasan, T.; Torrisi, F.; Popa, D.; Privitera, G.; Wang, F.; Bonaccorso, F.; Basko, D.M.; Ferrari, A.C. Graphene mode-locked ultrafast laser. *ACS Nano* **2010**, *4*, 803–810. [[CrossRef](#)] [[PubMed](#)]
6. Sotor, J.; Sobon, G.; Abramski, K.M. Scalar soliton generation in all-polarization-maintaining, graphene mode-locked fiber laser. *Opt. Lett.* **2012**, *37*, 2166–2168. [[CrossRef](#)]
7. Bouma, B.E.; Nelson, L.E.; Tearney, G.J.; Jones, D.J.; Brezinski, M.E.; Fujimoto, J.G. Optical coherence tomographic imaging of human tissue at 1.55 μm and 1.8 μm using Er-and Tm-doped fiber sources. *J. Biomed. Opt.* **1998**, *3*, 76–79. [[CrossRef](#)]
8. Hendow, S.T.; Shakir, S.A. Structuring materials with nanosecond laser pulses. *Opt. Express* **2010**, *18*, 10188–10199. [[CrossRef](#)]
9. Keller, U. Recent developments in compact ultrafast lasers. *Nature* **2003**, *424*, 831–838. [[CrossRef](#)]
10. Haris, H.; Baturalay, M.; Tan, S.J.; Markom, A.M.; Muhammad, A.R.; Harun, S.W.; Megat Hasnan, M.M.I.; Saad, I. Mode-Locked YDFL Using Topological Insulator Bismuth Selenide Nanosheets as the Saturable Absorber. *Crystals* **2022**, *12*, 489. [[CrossRef](#)]
11. Haris, H.; Muhammad, A.; Tan, S.; Markom, A.; Harun, S.; Hasnan, M.M.; Saad, I. Generation of Kelly and dip type sidebands soliton employing Topological insulator (Bi_2Te_3) as saturable absorber. *Infrared Phys. Technol.* **2022**, *123*, 104154. [[CrossRef](#)]
12. Shang, X.; Xu, N.; Zhang, H.; Li, D. Nonlinear photoresponse of high damage threshold titanium disulfide nanocrystals for Q-switched pulse generation. *Opt. Laser Technol.* **2022**, *151*, 107988. [[CrossRef](#)]
13. Zhao, R.; Li, J.; Zhang, B.; Li, X.; Su, X.; Wang, Y.; Lou, F.; Zhang, H.; He, J. Triwavelength synchronously mode-locked fiber laser based on few-layered black phosphorus. *Appl. Phys. Express* **2016**, *9*, 092701. [[CrossRef](#)]
14. Sun, X.; Nie, H.; He, J.; Zhao, R.; Su, X.; Wang, Y.; Zhang, B.; Wang, R.; Yang, K. Passively mode-locked 1.34 μm bulk laser based on few-layer black phosphorus saturable absorber. *Opt. Express* **2017**, *25*, 20025–20032. [[CrossRef](#)]
15. Wu, Q.; Jin, X.; Chen, S.; Jiang, X.; Hu, Y.; Jiang, Q.; Wu, L.; Li, J.; Zheng, Z.; Zhang, M. MXene-based saturable absorber for femtosecond mode-locked fiber lasers. *Opt. Express* **2019**, *27*, 10159–10170. [[CrossRef](#)] [[PubMed](#)]
16. Shi, Y.; Xu, N.; Wen, Q. Ti_2CT_x ($T=\text{O}, \text{OH}$ or F) nanosheets as new broadband saturable absorber for ultrafast photonics. *J. Light. Technol.* **2020**, *38*, 1975–1980. [[CrossRef](#)]
17. Bao, X.; Mu, H.; Chen, Y.; Li, P.; Li, L.; Li, S.; Qasim, K.; Zhang, Y.; Zhang, H.; Bao, Q. Ytterbium-doped fiber laser passively mode locked by evanescent field interaction with $\text{CH}_3\text{NH}_3\text{SnI}_3$ perovskite saturable absorber. *J. Phys. D Appl. Phys.* **2018**, *51*, 375106. [[CrossRef](#)]
18. Xu, N.; Sun, S.; Shang, X.; Zhang, H.; Li, D. Harmonic and fundamental-frequency mode-locked operations in an Er-doped fiber laser using a $\text{Cr}_2\text{Si}_2\text{Te}_6$ -based saturable absorber. *Opt. Mater. Express* **2022**, *12*, 166–173. [[CrossRef](#)]
19. Pang, L.; Sun, Z.; Zhao, Q.; Wang, R.; Yuan, L.; Wu, R.; Lv, Y.; Liu, W. Ultrafast Photonics of Ternary $\text{Re}_x\text{Nb}_{(1-x)}\text{S}_2$ in Fiber Lasers. *ACS Appl. Mater. Interfaces* **2021**, *13*, 28721–28728. [[CrossRef](#)]
20. Xu, J.; Liu, J.; Wu, S.; Yang, Q.H.; Wang, P. Graphene oxide mode-locked femtosecond erbium-doped fiber lasers. *Opt. Express* **2012**, *20*, 15474–15480. [[CrossRef](#)]
21. Wu, J.; Jia, L.; Zhang, Y.; Qu, Y.; Jia, B.; Moss, D.J. Graphene oxide for integrated photonics and flat optics. *Adv. Mater.* **2021**, *33*, 2006415. [[CrossRef](#)]
22. Huang, X.-M.; Liu, L.-Z.; Zhou, S.; Zhao, J.-J. Physical properties and device applications of graphene oxide. *Front. Phys.* **2020**, *15*, 33301. [[CrossRef](#)]
23. Park, S.; Ruoff, R.S. Chemical methods for the production of graphenes. *Nat. Nanotechnol.* **2009**, *4*, 217–224. [[CrossRef](#)] [[PubMed](#)]
24. Dideikin, A.T.; Vul', A.Y. Graphene oxide and derivatives: The place in graphene family. *Front. Phys.* **2019**, *6*, 149. [[CrossRef](#)]
25. Xing, G.; Guo, H.; Zhang, X.; Sum, T.C.; Huan, C.H.A. The physics of ultrafast saturable absorption in graphene. *Opt. Express* **2010**, *18*, 4564–4573. [[CrossRef](#)]
26. Sobon, G.; Sotor, J.; Jagiello, J.; Kozinski, R.; Zdrojek, M.; Holdynski, M.; Paletko, P.; Boguslawski, J.; Lipinska, L.; Abramski, K.M. Graphene oxide vs. reduced graphene oxide as saturable absorbers for Er-doped passively mode-locked fiber laser. *Opt. Express* **2012**, *20*, 19463–19473. [[CrossRef](#)] [[PubMed](#)]
27. Hummers, W.S., Jr.; Offeman, R.E. Preparation of graphitic oxide. *J. Am. Chem. Soc.* **1958**, *80*, 1339. [[CrossRef](#)]
28. Ferrari, A.C.; Meyer, J.C.; Scardaci, V.; Casiraghi, C.; Lazzeri, M.; Mauri, F.; Piscanec, S.; Jiang, D.; Novoselov, K.S.; Roth, S.; et al. Raman spectrum of graphene and graphene layers. *Phys. Rev. Lett.* **2006**, *97*, 187401. [[CrossRef](#)] [[PubMed](#)]
29. Ferrari, A.C.; Basko, D.M. Raman spectroscopy as a versatile tool for studying the properties of graphene. *Nat. Nanotechnol.* **2013**, *8*, 235. [[CrossRef](#)] [[PubMed](#)]
30. Kudin, K.N.; Ozbas, B.; Schniepp, H.C.; Prud'Homme, R.K.; Aksay, I.A.; Car, R. Raman spectra of graphite oxide and functionalized graphene sheets. *Nano Lett.* **2008**, *8*, 36–41. [[CrossRef](#)]

31. Lau, K.Y.; Liu, X.; Qiu, J. A Comparison for Saturable Absorbers: Carbon Nanotube Versus Graphene. *Adv. Photonics Res.* **2022**, 2200023. [[CrossRef](#)]
32. Zhao, J.; Wang, Y.; Yan, P.; Ruan, S.; Zhang, G.; Li, H.; Tsang, Y.H. An L-band graphene-oxide mode-locked fiber laser delivering bright and dark pulses. *Laser Phys.* **2013**, *23*, 075105. [[CrossRef](#)]
33. Xu, J.; Wu, S.; Li, H.; Liu, J.; Sun, R.; Tan, F.; Yang, Q.-H.; Wang, P. Dissipative soliton generation from a graphene oxide mode-locked Er-doped fiber laser. *Opt. Express* **2012**, *20*, 23653–23658. [[CrossRef](#)] [[PubMed](#)]
34. Lee, J.; Koo, J.; Debnath, P.; Song, Y.; Lee, J. A Q-switched, mode-locked fiber laser using a graphene oxide-based polarization sensitive saturable absorber. *Laser Phys. Lett.* **2013**, *10*, 035103. [[CrossRef](#)]
35. Tsai, L.-Y.; Li, Z.-Y.; Lin, J.-H.; Song, Y.-F.; Zhang, H. Wavelength tunable passive-mode locked Er-doped fiber laser based on graphene oxide nano-platelet. *Opt. Laser Technol.* **2021**, *140*, 106932. [[CrossRef](#)]
36. Liu, Z.-B.; He, X.; Wang, D. Passively mode-locked fiber laser based on a hollow-core photonic crystal fiber filled with few-layered graphene oxide solution. *Opt. Lett.* **2011**, *36*, 3024–3026. [[CrossRef](#)] [[PubMed](#)]
37. Li, X.; Tang, Y.; Yan, Z.; Wang, Y.; Meng, B.; Liang, G.; Sun, H.; Yu, X.; Zhang, Y.; Cheng, X. Broadband saturable absorption of graphene oxide thin film and its application in pulsed fiber lasers. *IEEE J. Sel. Top. Quantum Electron.* **2014**, *20*, 441–447.
38. Markom, A.; Tan, S.; Haris, H.; Paul, M.; Dhar, A.; Das, S.; Harun, S. Experimental Observation of Bright and Dark Solitons Mode-Locked with Zirconia-Based Erbium-Doped Fiber Laser. *Chin. Phys. Lett.* **2018**, *35*, 024203. [[CrossRef](#)]

Disclaimer/Publisher’s Note: The statements, opinions and data contained in all publications are solely those of the individual author(s) and contributor(s) and not of MDPI and/or the editor(s). MDPI and/or the editor(s) disclaim responsibility for any injury to people or property resulting from any ideas, methods, instructions or products referred to in the content.